ACS APPLIED MATERIALS & INTERFACES

Research Article

www.acsami.org

Electrorheology of Graphene Oxide

Wen Ling Zhang,[†] Ying Dan Liu,[†] Hyoung Jin Choi,*[,†] and Sang Guk Kim[‡]

[†]Department of Polymer Science and Engineering, Inha University, Incheon 402-751, Korea

[‡]Clean Fuel Department, Korea Institute of Energy Research, Daejon 305-343, Korea

Supporting Information

ABSTRACT: Novel polarizable graphene oxide (GO) particles with oxidized groups on their edge and basal planes were prepared by a modified Hummers method, and their electro-responsive electrorheological (ER) characteristics when dispersed in silicone oil were examined with and without an electric field applied. The fibrillation phenomenon of this GO-based electro-responsive fluid was also observed via an optical microscope under an applied electric field. Both flow curves and dielectric spectra of the ER fluid were measured using a rotational rheometer and a LCR meter, respectively. Its viscoelastic properties of both storage and loss moduli were also examined using a vertical oscillation rheometer equipped with a high voltage generator, finding that the GO-based smart ER system behaves as a viscoelastic material under an applied electric field.

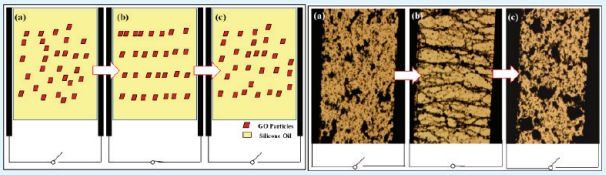

KEYWORDS: *electrorheological fluid, graphene oxide, vertical oscillation rheometer, suspension, rheology, dielectric property*

1. INTRODUCTION

Graphene is an individual and two-dimensional sheet of sp^2-bonded carbon which has been viewed as the mother of all other graphitic carbon materials of fullerene, carbon nanotube, and the most common graphitic form, graphite.[1] Since its first discovery, graphene has become an important material with its many potential and practical applications, such as touch display, electronic devices, transparent conducting films, catalyst supports, and capacitors.[2,3] Due to excellent properties of graphene such as its unique electronic characteristics, good mechanical strength, exceptional thermal conductivity, and high specific surface area,[4,5] its facile synthesis and commercial application has been a hot topic of conversation.[6,7]

In this work, the oxidized graphite (graphite oxide) was used to deal with the synthetic issue of graphene first. Graphite oxide is an interesting material because of its excellent dispersion stability in water and other common organic solvents such as acetone, methanol, ethanol, etc.[8,9] Unlike graphite, the dispersed state of graphite oxide can be exfoliated to graphene oxide (GO) by sonication.[10]

Meanwhile low electrical conductivity of the GO compared to that of graphene has been a major obstacle factor which hinders its application as a conducting material, and it thus needs to be treated in hydrazine hydrate vapor or with high heat to improve its electrical conductivity.[11,12] Nonetheless, the low electrical conductivity of the GO becomes a favorable factor in this study for its application as an electrorheological (ER) smart material to avert an electrical short circuit problem, in which the ER fluids are in general composed of polarizable particles dispersed in insulating medium oils such as mineral oil, silicone oil, and corn oil.[13−15]

By combining suitable electrical conductivity and high dielectric constant property into the GO-based composites for an ER material with tunable conductivity and well dispersion properties of the GO owing to its functional groups, we recently reported conducting polyaniline/GO composite,[16] titania/GO composite,[17] and GO coated core−shell structured polystyrene microspheres[18] as ER materials. Other graphene-based materials like polyaniline decorated graphene sheet was also reported recently as ER smart materials.[19] However, compared with these GO-based composites for the ER fluid, the outstanding advantage of the GO-based ER fluid is not only with its ER effect but also with its simplicity, time-savings, and mass producibility. Note that an additional dedoping process has to be carried out in the case of polyaniline(PANI)/GO-based ER fluid due to the high electrical conductivity of polyaniline itself as well as the titania particle surface has to be modified prior to the preparation of GO/titania composite.

Since the ER fluids vary in their rheological properties under applied electric field strength and exhibit rapid microstructural transition from a fluid-like to a solid-like state within a millisecond, they have been extensively studied because of their potential applications in many industrial areas such as torque transducers, vibration attenuators, control systems, and ER polishing.[20,21] In this study, rheological characteristics of flow curves and shear viscosity along with dielectric spectra of the GO-based ER fluid were measured using a rotational rheometer and a LCR meter, respectively. Another interesting property from its particle chain structure formation is its viscoelasticity. The custom designed vertical oscillation rheometer (VOR) was used for acquiring rheological parameters from a dynamic test of the ER fluid. The synthesized two-dimensional GO material

Received: February 15, 2012
Accepted: April 4, 2012
Published: April 4, 2012

was also characterized by scanning electron microscopy (SEM), transmission electron microscopy (TEM), X-ray diffraction (XRD), Fourier transform infrared spectroscopy (FT-IR), thermo gravimetric analysis (TGA), and X-ray photoelectron spectroscopy (XPS).

2. EXPERIMENTAL SECTION

2.1. Materials. Raw materials of graphite (powder, <45 μm, ≥99.99%, Sigma-Aldrich) and all the chemical reagents of strong oxidant $KMnO_4$ (Sigma-Aldrich), $NaNO_3$ (Junsei Co., Japan), 35% HCl (DC Chemical, Korea), and 98% H_2SO_4 (DC Chemical, Korea) were used as received without further purification. Di water was used in all the experimental processes and washing.

2.2. Preparation of Graphene Oxide (GO). Graphene oxide (GO) was fabricated from graphite powder by a modified Hummers method. In a typical synthesis procedure, 3 g of graphite powder was added to 210 mL of H_2SO_4 (98%) (in an ice bath), and then 9 g of $KMnO_4$ and 1.5 g of $NaNO_3$ were added gradually. The mixture was stirred continually for 4 h under an ice bath to keep the temperature at appropriately 22 °C, and then 200 mL of Di water was added to dilute the mixture; it was maintained at that temperature for 30 min. After that, a 30% H_2O_2 solution was added into the solution slowly while stirring until the color of suspension turned to brilliant brown, indicating full oxidization of graphite.

The as-obtained graphite oxide slurry was dispersed in Di water and exfoliated into the GO via sonication using an ultrasonic generator (28 kHz, 600 W, Kyungil Ultrasonic Co., Korea) for 3 h under stirring. The color of the suspension turned to black again due to the formation of GO sheets during ultrasonic treatment. Finally, the mixture was collected using a centrifuge, washed three times with 5% HCl, followed with Di water repeatedly until the pH = 7, and finally dried in a vacuum oven at 120 °C for 3 days.

2.3. Preparation of ER Fluid. The GO powders were shook through a sieve (100 μm) to separate large particles and stored in an oven at 60 °C for 24 h before being used. The ER fluid was prepared by dispersing GO particles in a silicone oil (100 cS, 0.965 g/cm^3) by sonication to obtain good dispersion (5 wt %, volume fraction = 2.77%). The fibrillation phenomenon was observed under an optical microscopy with a DC high voltage source which was used to apply a voltage. Gap distance between the two parallel electrodes was 300 μm.

2.4. Characterization. Morphologies of both pure graphite and GO were observed by a scanning electron microscope (SEM) with an applied voltage of 15 kV at a work distance of 15 mm (SEM, S-4300, Hitachi, Japan) and a transmission electron microscope (TEM) (Philips CM200). The crystal structures of the samples were indicated using an X-ray diffractometer (DMAX-2500, Rigaku). Thermal properties were examined by the thermal gravimetric analyzer (TGA) (TA Instruments, Q50, USA), in which the samples were heated from room temperature to 750 at 5 °C/min under a nitrogen flow. Electron spectroscopy for chemical analysis (XPS) measurements was presented using the analyzer (K-Alpha, Thermo Scientific). The electrical conductivity was measured using a 4-pin probe resistivity meter (QPP, Loresta-GP, Mitsubishi Chem. Co.), while the density of GO was obtained using a gas pycnometer. A fibrillation phenomenon of the GO-based ER fluid was directly observed by an optical microscope (OM) (Olympus BX 51). The flow behaviors of shear stress as a function of shear rate for different applied electric fields were investigated by a rotational rheometer (Physica MC300, Germany) equipped with a high voltage generator using a Couette-type sample loading geometry with a bob and cup (CC 17, gap distance is 0.71 mm) in which the data were obtained with an experimental error range of ±5.0%. The dielectric spectra of ER fluid were also measured using the LCR meter (Hewlett-Packard HP 4284A) with a liquid measuring fixture (HP 16452A) to investigate their interfacial polarization within the frequency range from 20 Hz to 1 MHz. A custom designed VOR was used to measure rheological properties of the ER fluid. This rheometer can control the amplitude of the strain in the range from 0.003 to 1 and the frequency in the range from 0.1 to 100 Hz. Raw data from the VOR were obtained from the oscilloscope voltage signals (both an input strain and an output force wave), in which we repeated the rheometer measurements three times to make sure that the data are credible within the error range of ±4.8%.

3. RESULTS AND DISCUSSION

The SEM images of both pure graphite (left) and GO (right) were shown in Figure S1a,b, respectively, Supporting Information. Compared to the pure graphite, the GO displays clearly different morphology. The obvious flakey structure disappeared after oxidation, and the fact that GO surface became darker than that of pure graphite may be due to the introduced functional groups on its edges. Energy dispersive X-ray spectroscopy (EDX) analyses of the two samples are shown in Figure S1c,d, respectively, Supporting Information. As shown in Figure S1c, Supporting Information, the element of C (83.60%) is in the majority in pure graphite. Compared with the EDX spectra of pure graphite, the composition of oxygen increased from 4.45 to 31.72 wt %, indicating the success of adding oxidative functional groups on graphene surface. Moreover, the Pt element in both pure graphite and GO is

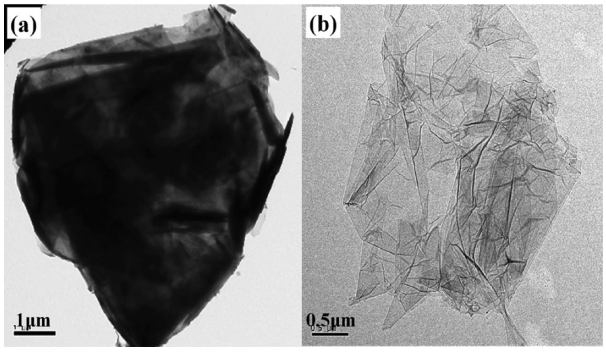

Figure 1. TEM images of (a) pure graphite and (b) GO.

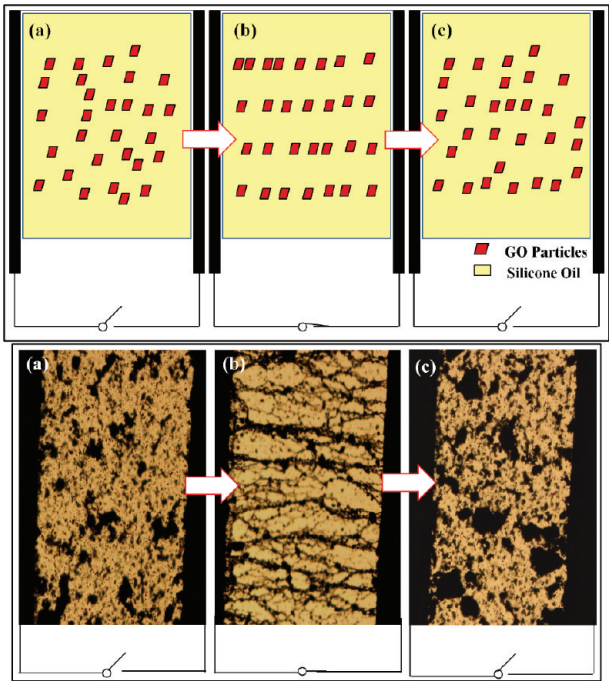

Figure 2. OM images of GO particles dispersed in silicone oil without (a), with (b), and without (c) the electric field.

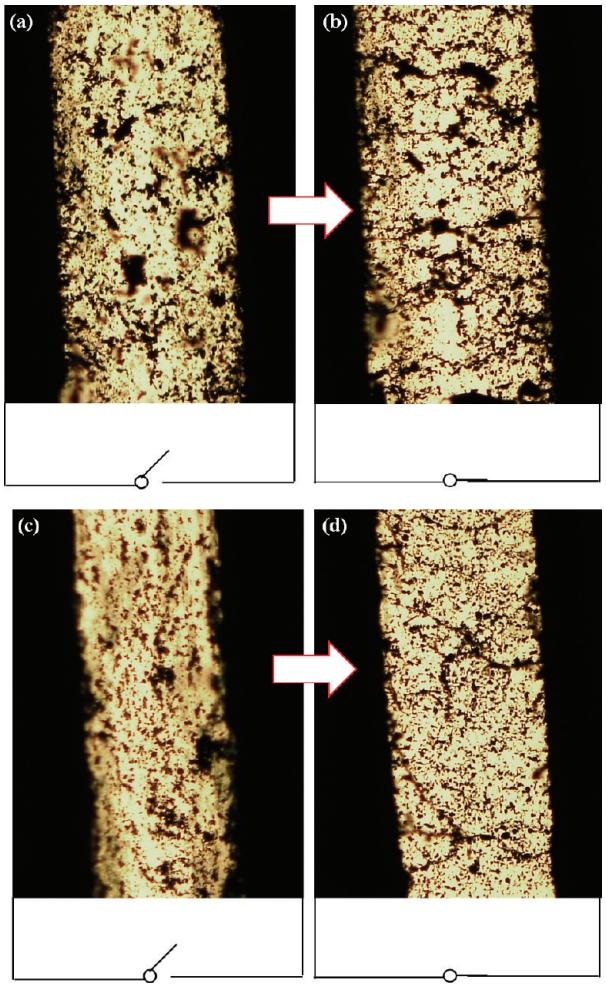

Figure 3. OM images of graphene and graphite particles dispersed in silicone oil without (a, c) and with an electric field (b, d).

an impurity, and the elements of Si and S in GO are due to an oxidized process.

The TEM images of both pure graphite and GO are illustrated in Figure 1a,b, respectively. Pure graphite in Figure 1a shows dark and opaque morphology; as a sharp contrast, the GO image is transparent, confirming that the successful exfoliation of graphite via sonication occurred as shown in Figure 1b.

The XRD data can confirm the structural differences between pure graphite and GO further as shown in Figure S2, Supporting Information. A strong peak of pure graphite was shown at $2\theta = 26.32°$, while the peak of GO was much reduced and shown at $2\theta = 11.79°$. According to Bragg's law, $n\lambda = 2d \sin \theta$, where n is an integer, θ is the angle of incidence (or reflection) of the X-ray beam, and λ is the X-ray wavelength (in the case of Cu Kα1 radiation, $\lambda = 0.154$ nm); the interlayer distance between GO layers was much enlarged from 0.34 to 0.75 nm, clearly demonstrating that the GO was fully exfoliated to graphene sheets via sonication.[22]

The successful addition of oxidized groups onto the graphene edges reflected the TGA curves. Figure S3, Supporting Information, shows the TGA traces of pure graphite and GO which were heated in a TGA instrument to 750 °C at a heating rate of 5 °C/min under N_2. Little weight loss is defected when pure graphite is heated up to 750 °C. Compared with the raw graphite, GO seems to be much more thermally unstable. The

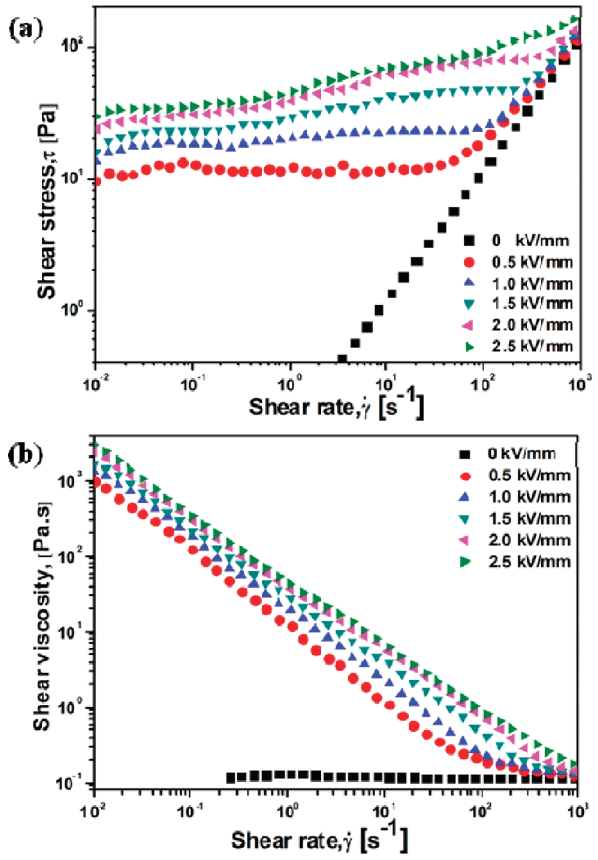

Figure 4. Shear stress (a) and shear viscosity (b) of 5 wt % GO-based ER fluid as a function of shear rate under different electric fields.

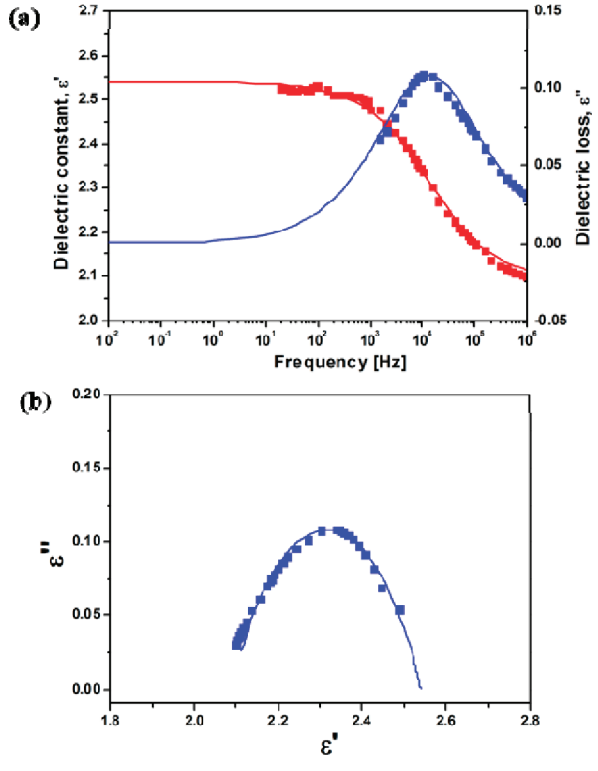

Figure 5. Dielectric spectra (a) and Cole−Cole fitting curves (b) of 5 wt % GO-based ER fluid.

dx.doi.org/10.1021/am300267f | ACS Appl. Mater. Interfaces 2012, 4, 2267−2272

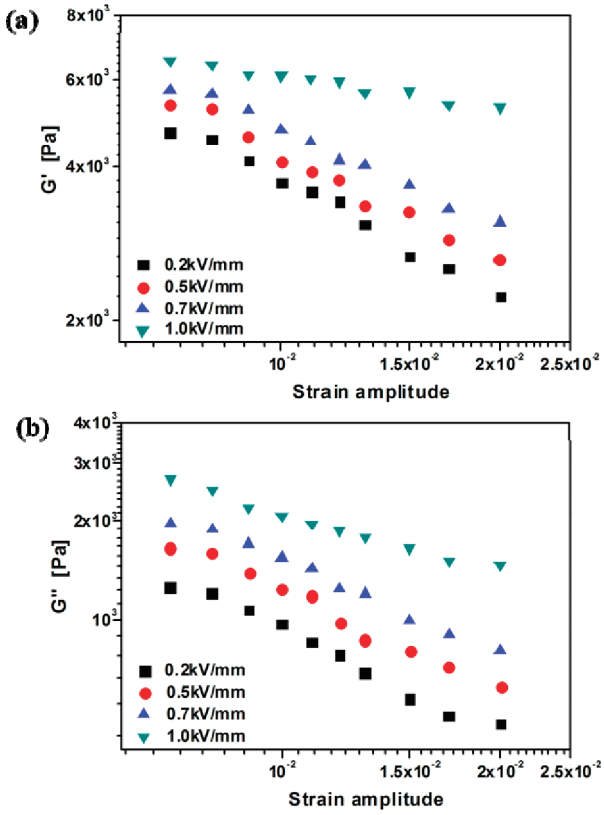

Figure 6. Storage modulus G' (a) and loss modulus G'' (b) as a function of strain amplitude measured by VOR for a 5 wt % GO dispersed in 100 cS silicone oil at different electric field strengths and a frequency of 3 Hz.

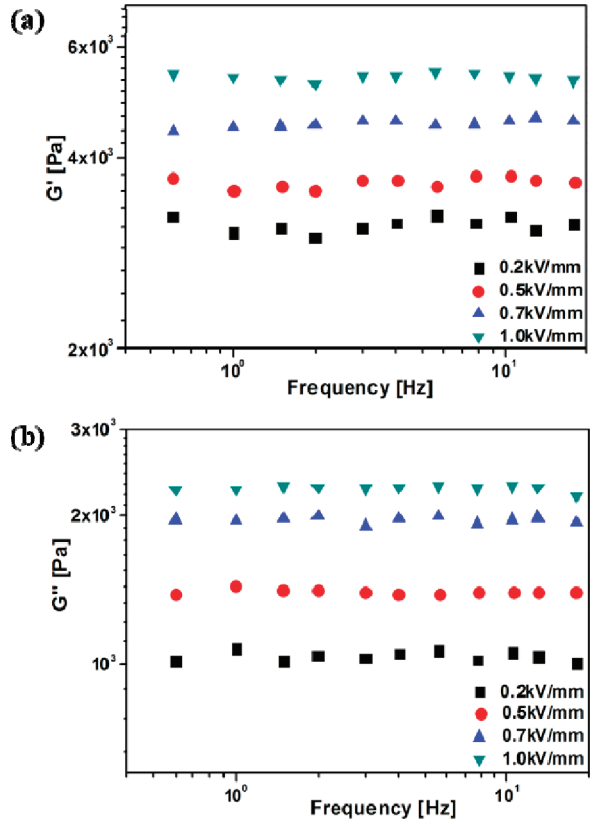

Figure 7. G' (a) and G'' (b) values in a frequency sweep test under various electric field strengths.

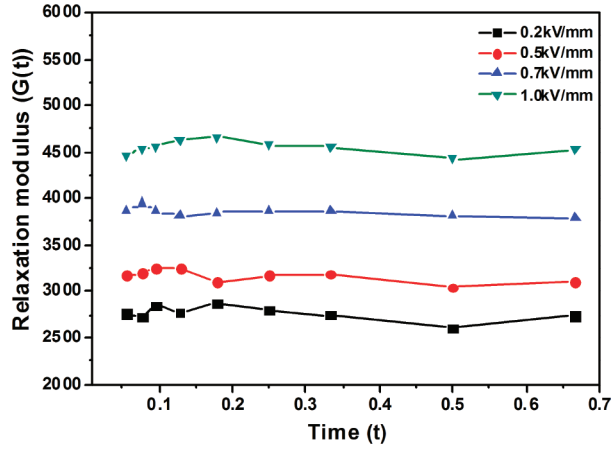

Figure 8. Relaxation modulus $G(t)$ of 5 wt % GO dispersed in 100 cS silicone oil, calculated from $G'(\omega)$ and $G''(\omega)$.

main mass loss takes place around 150−300 °C due to the pyrolysis of oxygen functional groups thereby weakening the van der Waals forces between layers.[23,24] A mass loss below 100 °C which is attributed to the removal of adsorbed water was also observed.

We employed X-ray photoelectron spectroscopy (XPS) to analyze the type and number of different interactions of pure graphite and GO. Figure S4, Supporting Information, shows the C1s and O1s spectra and survey data which were collected on pure graphite and GO dry powders. The C1s region of pure graphite showed primary binding energies at 284.53 (C═C) (69.16%) and few oxidized binding energies at 285.94 (C−OH) (12.03%) and 288.49 (C═O) (6.5%); on the other hand, GO showed a large number of oxidized binding energies at 287.42 (C═O) (34.01%), 285.41 (C−OH) (29.37%), 288.27 eV(O−C═O) (22.15%), and 286.15 eV(C−O) (14.24%).[25] We can depict obviously that the percent of oxygen was enlarged after oxidation which indicates the success of adding oxidized functional groups on the graphene edge.

The electrical conductivity of obtained GO is 6.02×10^{-6} S/cm. The dilute ER fluid (volume fraction = 2.77%) was prepared by dispersing the GO powder in 100 cS silicone oil. The GO particle sheets were grinded by mill, sieved (sieve 100 μm) carefully, and then stored in oven at 60 °C for 24 h before used. The density of obtained GO powders is 1.78 g/cm^3. The ER fluid was dropped between two parallel electrodes (distance is 300 μm), and the optical microscopic (OM) images of GO-based ER fluid were captured when the electric field (0.67 kV/mm) is off (Figure 2a), on (Figure 2b), and off (Figure 2c), sequentially. We can clearly see that the ER fluid particles move randomly (Figure 2a), while the dispersed GO particles form a chain-like structure, indicating a solid-like behavior as soon as the electric field is applied (Figure 2b).[26−28] It is interesting to see that the previously formed chain-like structures deform and the particles move randomly when the electric field is turned off, showing the reversible behavior of ER effect as demonstrated in Figure 2c. Note that such a chain-like structure has been also observed for carbon nanotube coated polymer bead and polyaniline/GO nanocomposite systems.[29]

For further observation of the chain formation characteristics of the GO as a function of electric field strengths, we applied different electric fields and captured the various chain-like structures as shown in Figure S5, Supporting Information,

dx.doi.org/10.1021/am300267f | ACS Appl. Mater. Interfaces 2012, 4, 2267−2272

(0.33, 0.67, 1.0, and 1.33 kV/mm). The ER fluid formed stronger chains when a higher electric field was imposed.

To compare the ER properties with and without polar groups such as hydroxyl, epoxide, and carboxyl groups, we dispersed the graphite and graphene powders in silicone oil and observed them using an OM without and with an applied electric field (0.67 kV/mm) as shown in Figure 3a,c and in Figure 3b,d, respectively. Compared with the obvious fibrillar structure in the GO-based ER fluid, tiny structural changes when the electric field is applied in both graphene and graphite suspensions are detected, confirming the conjecture that the polar functional groups (like hydroxyl, epoxide, and carboxyl groups) on carbon backbone could strengthen the ER activity.

The ER characteristics for 5 wt % of GO-based ER fluid were measured from a controlled shear rate (CSR) test mode using a Couette-type rotational rheometer equipped with a high voltage generator. As presented in Figure 4, the flow curves of shear stress and shear viscosity were examined as a function of applied electric field. Figure 4a showed the GO-based ER fluid exhibits typical ER behavior. Without an external electric field, the fluid behaved similar to a Newtonian fluid, in which the shear stress increased linearly (the slope close to 1) with increasing shear rates. In contrast, when exposed to a high electric field, the particles were polarized and formed chain-like structures, as shown in the OM images and exhibited a large increase in their shear stresses.[30] However, compared to previously reported PANI/GO-based ER fluid which shows typical ER characteristics with a large increase of shear stress for different electric fields,[31] the increase of shear stress for different electric fields for the GO-based ER fluid was not significant. This might come from the mechanically flexible GO sheets which is weaker than the mechanical strength of PANI/GO composite particle. The shear viscosity as a function of the shear rate was shown in Figure 4b. Compared to the uniform viscosity at E = 0 kV/mm of a Newtonian-like fluid, typical shear thinning behaviors coming from their solid-like characteristics were observed under different electric fields.

On the other hand, dielectric constant (ε') and dielectric loss (ε'') are other important physical parameters for ER suspensions regarding their polarization. Figure 5a,b shows the dielectric spectra (ε', ε'') as a function of the frequency (from 20 Hz to 1 MHz) and Cole−Cole plots for 5 wt % GO-based ER fluid, respectively. The lines in Figure 5 are fitted from the following well-known Cole−Cole formula:[32]

$$\varepsilon^* = \varepsilon' + i\varepsilon'' = \varepsilon_\infty + \frac{\Delta\varepsilon}{1 + (i\omega\lambda)^{1-\alpha}} \quad (1)$$

Here, ε_0 is the dielectric constant when the frequency ω is close to 0 and ε_∞ is the dielectric constant at a high frequency limit. $\Delta\varepsilon = \varepsilon_0 - \varepsilon_\infty$ is the achievable polarizability of an ER fluid which is related to the electrostatic interaction between particles, while the exponent $(1 - \alpha)$ characterizes the broadness of the relaxation time distribution. The relaxation time, $\lambda = 1/2\pi f_{max}$, reflects the rate of interfacial polarization when an electric field is applied, where f_{max} is the maximum of the dielectric loss of an ER fluid. Note that the higher stress enhancement is achieved when the λ becomes smaller within the adequate range and the bigger $\Delta\varepsilon$ is applied.

From its fitting result, the values of α, λ, ε_0, and ε_∞ are estimated to be 0.428, 0.000013, 2.54, and 2.09, respectively, indicating that an amazingly fast polarization response of the particles under an applied electric field results in its effectiveness to good ER performance. Furthermore, the VOR has been adopted for a dynamic test of the ER fluids especially which possess relatively high electrical conductivity, thus easily inducing an electrical short problem when commercial rheometers are used. The equipment consists of three parts as shown in Figure S6, Supporting Information: a measuring unit, a deformation inducting unit, and a force-detecting unit with an oscilloscope for the data processing. The measuring unit is composed of an inner cylinder and an out cup, where the ER fluid sample is placed in this unit and is connected to a high voltage generator. In the upside of the inner cylinder, an air vent is placed to reduce the experimental error generated by the air between the sample and the inner cylinder. The deformation input part consists of a function generator, a powder amplifier, and and actuator (speaker) connected to the inner cylinder. The output part is composed of the proximeter for strain, a load cell for force, and an oscilloscope. The detailed principle about VOR can be found in our previous work.[33]

A transducer technique with a load cell is used to convert the output compression and tension forces to a voltage signal. In order to transform the voltage to a force, the linear relationship between the force and voltage is calibrated as shown in Figure S7, Supporting Information.

In the measuring unit, the inner cylinder moves up and down with the actuator while the outer cup is stationary. Because both the inside of the inner cylinder and the bottom of the cup are insulated, the electric field is only applied in the gap of the measuring unit. We can also control both the frequency in the range from 0.1 to 100 Hz and the magnitude of deformation from a function generator to the speaker amplifier. The ER sample is deformed as the inner cylinder vibrated, and the resulting force is transferred to the cup. The input strain and output force can be observed from the oscilloscope voltage signals from the proximeter and load cell, respectively. From these input and output signals, the phase angle (δ), the frequency (ω), the amplitude of the strain (z_0), and the maximum force (F_0) are obtained. The viscoelastic parameters (G', G'', and tan δ) can be calculated from the following equations:[34]

$$G' = \frac{F_0 \cos\delta \ln a}{2\pi l z_0}$$

$$G'' = \frac{F_0 \sin\delta \ln a}{2\pi l z_0}$$

$$\tan\delta = \frac{G''}{G'} \quad (2)$$

where a is the ratio of the inner cylinder and the outer cup radii, F_0 is the magnitude of the force, and l is the height of the inner cylinder. The inner cylinder is 20 mm in diameter and 19 mm in depth, while the outer cup is 22 mm in diameter and 29 mm in depth.

Figure 6 represents storage modulus G' (panel a) and loss modulus G'' (panel b) as a function of strain amplitude for the GO-based ER fluid at a frequency of 3 Hz under different electric fields using the VOR. Both the G' and G'' increased with the electric field strength over the entire range of strain.[34]

Figure 7 represents the results of G' and G'' as a function of frequency at a critical strain of 0.007 in the range of a linear viscoelastic region from Figure 6 in the range from 0.1 to 20 Hz under different electric fields. Both G' and G'' increase significantly with the electric field strength over the entire

range of frequency due to the increased interparticle force. The G' exhibits a plateau over a broad frequency range so that we can clearly observe that the GO-based ER fluid behaves like a viscoelastic solid in the linear viscoelastic region due to the formation of particle chain structure. In addition, G'' is observed to be lower than that of G' under the same frequency, confirming the solid-like property of the ER fluid further.

In order to analyze the phase change from a liquid-like to a solid-like phase, we calculated the stress relaxation modulus $G(t)$ from the values of $G'(\omega)$ and $G''(\omega)$ using the Schwarzl equation[35] given in eq 3. Note that the values of $G(t)$ are difficult to measure experimentally due to the intrinsic properties of materials and the limitation of mechanical measurements.[34] As shown in Figure 8, the $G(t)$ is nearly stable as a function of time on a log−log scale with increasing electric field strength, again employing its solid-like characteristics.

$$G(t) \cong G'(\omega) - 0.560G''(\omega/2) + 0.200G''(\omega) \quad (3)$$

4. CONCLUSION

Exfoliated graphite oxide of the GO was prepared via a modified Hummers method, and both SEM and TEM images showed morphological differences between pure graphite and GO. XRD and XPS data confirmed the presence of functional groups on graphene edges after an oxidized process. The GO possessed an appropriate electric conductivity as an ER smart material, in which the reversible chain-like structure was observed using an OM when dispersed in silicone oil under an electric field, demonstrating a typical ER behavior. To study its ER performance further, we also analyzed the flow response as a function of shear rate using a rotational rheometer and the dielectric spectra with the LCR meter. The GO-based ER fluid gets polarized and exhibits typical viscoelastic properties over a wide range of either strain or frequency under an electric field using a custom-designed VOR.

■ ASSOCIATED CONTENT

Ⓢ Supporting Information

Figures including SEM images of pure graphite, GO and their EDX spectra, XRD images, TGA curves, XPS spectra. OM images of GO particles dispersed in silicone oil under different electric fields from (a) to (d) (0.33, 0.67, 1.0, 1.33 kV/mm). Overall configuration of VOR, the relation between voltage and weight on the load cell. This information is available free of charge via the Internet at http://pubs.acs.org/.

■ AUTHOR INFORMATION

Corresponding Author

*E-mail: hjchoi@inha.ac.kr.

Notes

The authors declare no competing financial interest.

■ ACKNOWLEDGMENTS

This research was supported by a grant from the Fundamental R&D Program for Core Technology of Materials funded by the Ministry of Knowledge Economy, Korea (2011).

■ REFERENCES

(1) Wu, Y. H.; Yu, T.; Shen, Z. X. *J. Appl. Phys.* **2010**, *108*, 071301.
(2) Fang, M.; Long, L.; Zhao, W.; Wang, L.; Chen, G. *Langmuir* **2010**, *26*, 16771−16774.
(3) Bhunia, S. K.; Jana, N. R. *ACS Appl. Mater. Interfaces* **2011**, *3*, 3335−3341.
(4) Zhang, Y. B.; Tan, Y. W.; Stormer, H. L.; Kim, P. *Nature* **2005**, *438*, 201−204.
(5) Balandin, A. A.; Ghosh, S.; Bao, W. Z.; Calizo, I.; Teweldebrhan, D.; Miao, F.; Lau, C. N. *Nano Lett.* **2008**, *8*, 902−907.
(6) Eswaraiah, V.; Sankaranarayanan, V.; Ramaprabhu, S. *ACS Appl. Mater. Interfaces* **2011**, *3*, 4221−4227.
(7) Cote, L. J.; Kim, J.; Zhang, Z.; Sun, C.; Huang, J. *Soft Matter* **2010**, *6*, 6096−6101.
(8) McAllister, M. J.; Li, J. L.; Adamson, D. H.; Schniepp, H. C.; Abdala, A. A.; Liu, J.; Herrera-Alonso, M.; Milius, D. L.; Car, R.; Prud'homme, R. K.; Aksay, I. A. *Chem. Mater.* **2007**, *19*, 4396−4404.
(9) Stankovich, S.; Dikin, D. A.; Piner, R. D.; Kohlhaas, K. A.; Kleinhammes, A.; Jia, Y.; Wu, Y.; Nguyen, S. T.; Ruoff, R. S. *Carbon* **2007**, *45*, 1558−1565.
(10) Wang, G.; Shen, X.; Wang, B.; Yao, J.; Park, J. *Carbon* **2009**, *47*, 1359−1364.
(11) Gilje, S.; Han, S.; Wang, M.; Wang, K. L.; Kaner, R. B. *Nano Lett.* **2007**, *7*, 3394−3398.
(12) Si, Y.; Samulski, E. T. *Nano Lett.* **2008**, *8*, 1679−1682.
(13) Cheng, Y.; Wu, K.; Liu, F.; Guo, J.; Liu, X.; Xu, G.; Cui, P. *ACS Appl. Mater. Interfaces* **2010**, *2*, 621−625.
(14) Cheng, Q.; Pavlinek, V.; He, Y.; Yan, Y.; Li, C.; Saha, P. *Colloid Polym. Sci.* **2011**, *289*, 799−805.
(15) Hiamtup, P.; Sirivat, A.; Jamieson, A. M. *J. Mater. Sci.* **2010**, *45*, 1972−1976.
(16) Zhang, W. L.; Park, B. J.; Choi, H. J. *Chem. Commun.* **2010**, *46*, 5596−5598.
(17) Zhang, W. L.; Choi, H. J. *Chem. Commun.* **2011**, *47*, 12286−12288.
(18) Zhang, W. L.; Liu, Y. D.; Choi, H. J. *J. Mater. Chem.* **2011**, *21*, 6916−6921.
(19) Yin, Y.; Wang, X.; Chang, R.; Zhao, X. *Soft Matter* **2012**, *8*, 294−297.
(20) Tao, R.; Huang, K.; Tang, H.; Bell, D. *Energy Fuels* **2008**, *22*, 3785−3788.
(21) Zhang, M.; Gong, X.; Wen, W. *Electrophoresis* **2009**, *30*, 3116−3123.
(22) Du, X. S.; Yu, Z. Z.; Dasari, A.; Ma, J.; Mo, M. S.; Meng, Y. Z.; Mai, Y. W. *Chem. Mater.* **2008**, *20*, 2066−2068.
(23) Yang, H. F.; Li, F. H.; Shan, C. S.; Han, D. X.; Zhang, Q. X.; Niu, L.; Ivaska, A. *J. Mater. Chem.* **2009**, *19*, 4632−4638.
(24) Stankovich, S.; Dikin, D. A.; Piner, R. D.; Kohlhaas, K. A.; Kleinhammes, A.; Jia, Y.; Wu, Y.; Nguyen, S. T.; Ruoff, R. S. *Carbon* **2007**, *45*, 1558−1565.
(25) Yang, Y. F.; Wang, J.; Zhang, J.; Liu, J. C.; Yang, X. L.; Zhao, H. Y. *Langmuir* **2009**, *25*, 11808−11814.
(26) Cheng, Q.; Pavlink, V.; He, Y.; Li, C.; Saha, P. *Colloid Polym. Sci.* **2009**, *287*, 435−441.
(27) Choi, H. J.; Jhon, M. S. *Soft Matter* **2009**, *5*, 1562−1567.
(28) Yin, J.; Zhao, X.; Xiang, L.; Xia, X.; Zhang, Z. *Soft Matter* **2009**, *5*, 4687−4697.
(29) Shin, K.; Kim, D.; Cho, J. C.; Lim, H. S.; Kim, J. W.; Suh, K. D. *J. Colloid Interface Sci.* **2012**, *374*, 18−24.
(30) Yin, J. B.; Xia, X.; Wang, X. X.; Zhao, X. P. *Soft Matter* **2011**, *7*, 10978−10986.
(31) Zhang, W. L.; Liu, Y. D.; Choi, H. J. *Carbon* **2012**, *50*, 290−296.
(32) Cho, M. S.; Choi, H. J.; Ahn, W. S. *Langmuir* **2004**, *20*, 202−207.
(33) Choi, M. S.; Choi, Y. J.; Choi, H. J.; Kim, S. G.; Jhon, M. S. *J. Mol. Liq.* **1998**, *75*, 13−24.
(34) Kim, S. G.; Kim, J. W.; Cho., M. S.; Choi, H. J.; Jhon, M. S. *J. Appl. Polym. Sci.* **2001**, *79*, 108−114.
(35) Schwarzl, F. L. *Rheol. Acta* **1975**, *14*, 581−590.